Supplementary Materials for "Systematic assessment of the effects of space averaging and time averaging on weather forecast skill"

Ying Li and Samuel N. Stechmann

November 22, 2022

Abstract

This supplementary material includes three sections: (1) additional sensitivity tests, (2) a derivation of the analytical formula for the decorrelation time of the time-averaged stochastic process, and (3) figures of performance increase in terms of percentage increase via time averaging or space averaging.

1 Additional Sensitivity Tests

In this section, to test the robustness of the results in the main manuscript, additional sensitivity tests are implemented. One test involves using anomaly data (using anomalies from the seasonal cycle) where a long term smoothed seasonal cycle is subtracted from the original data for both precipitation and temperature. Beyond that, the average from the past 14 days to the future 14 days is used as a second version of seasonal cycle for the surface temperature in the second test. In the third test, the average from the past 14 days to the current time point serves as the seasonal cycle for the surface temperature. For precipitation, another dataset, the GPM (Global Precipitation Measurement) dataset, is used as the truth signal as an additional robustness test.

1.1 Analysis on anomaly data for precipitation and temperature

Forecast skill changes are now investigated in the GFS precipitation rate/surface temperature anomaly data. The anomaly data is defined by subtracting a smoothed seasonal cycle before assessing the forecast skills.

For the precipitation rate, the enhanced monthly long term mean CPC Merged Analysis of Precipitation (CMAP) is used for calculating the seasonal cycle. For the surface temperature, GFS analysis data with lead 0 are used. More details about the seasonal cycles are explained in the Method section of main manuscript.

The main results are shown in Fig. S1. In the comparison between forecast performance changes via time averaging vs. spatial averaging, essentially the same result is obtained: spatial averaging is more efficient than time averaging in improving the forecast skills, both for the precipitation and the temperature. One difference seen in Fig. S1b is that the temperature forecast skill is lower for the anomalies from the seasonal cycle, in comparison to the case of the main text, where the temperature forecast skills were higher. This difference indicates that variations from the seasonal cycle contribute a substantial amount of the forecast skill. Nevertheless, as seen in this additional test, the effects of time averaging vs. space averaging are essentially the same no matter the seasonal cycle is retained or removed or not.

1.2 Temperature anomaly data analaysis using centered 28 days average as the seasonal cycle

As another sensitivity test, the average from the past 14 days to the future 14 days of the surface temperature is used as the seasonal cycle for 3.5 months surface temperature data.

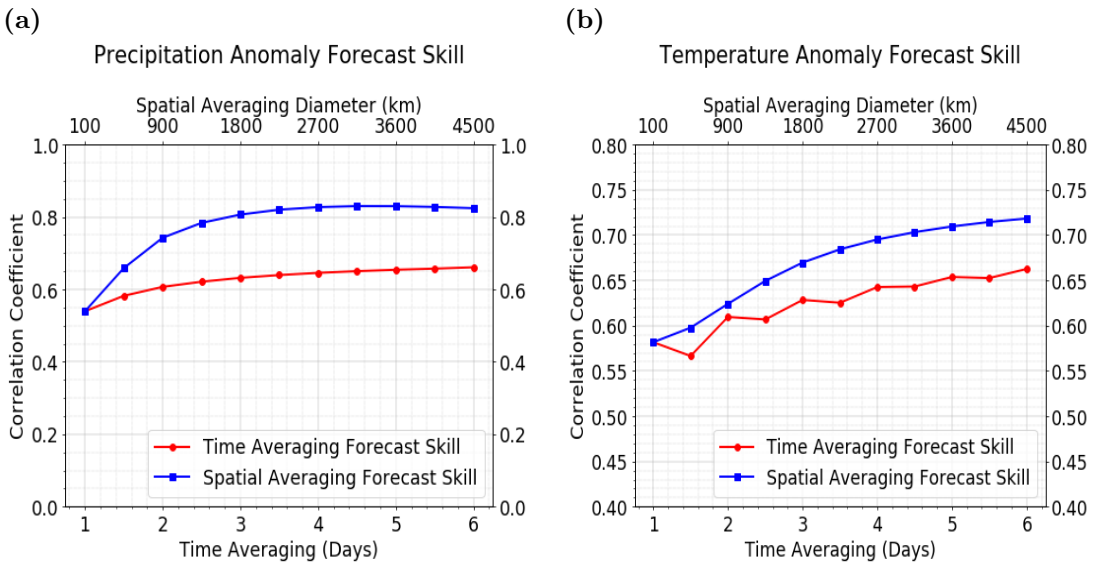

Figure S1: Effect of time and space averaging on forecast skill, averaged globally. **(a)** Precipitation anomaly, at a lead time of 3 days. (b) Surface temperature anomaly, at a lead time of 7 days.

The spatial averaging is still showing a much better effect in improving the forecast performance than time averaging from the new global map.

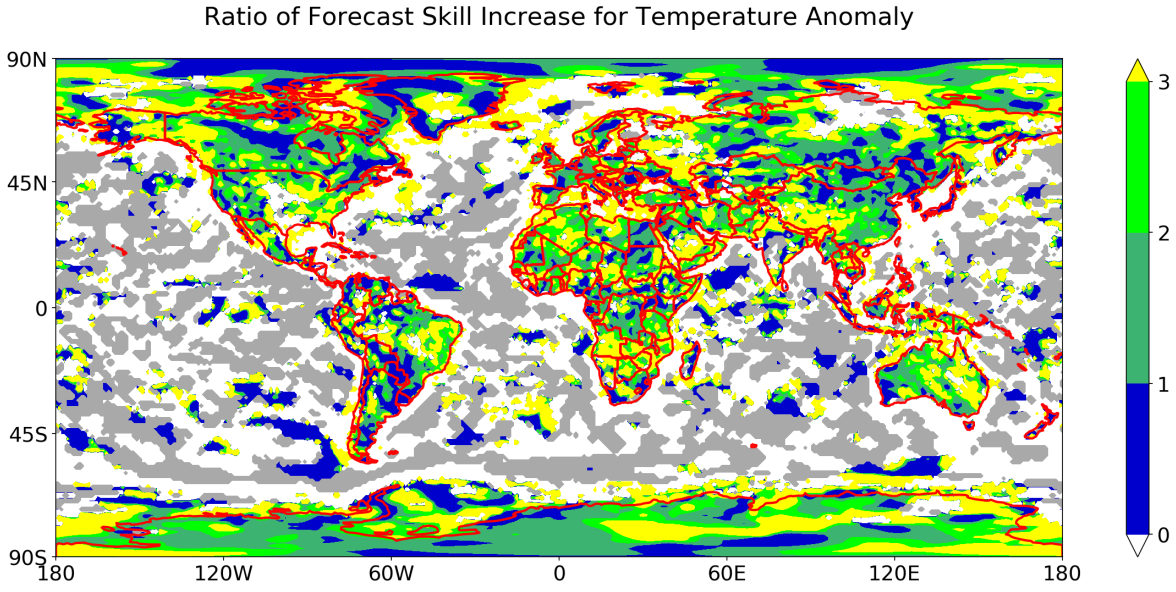

Figure S2: Global map of the ratio of forecast skill increase, defined as $r = \Delta_x \rho / \Delta_t \rho$, where $\Delta_x \rho$ is the change in forecast skill due to increased spatial averaging, and $\Delta_t \rho$ is the change in forecast skill for increased time averaging for surface temperature anomaly using the average from the past 14 days to the future 14 days as the seasonal cycle.

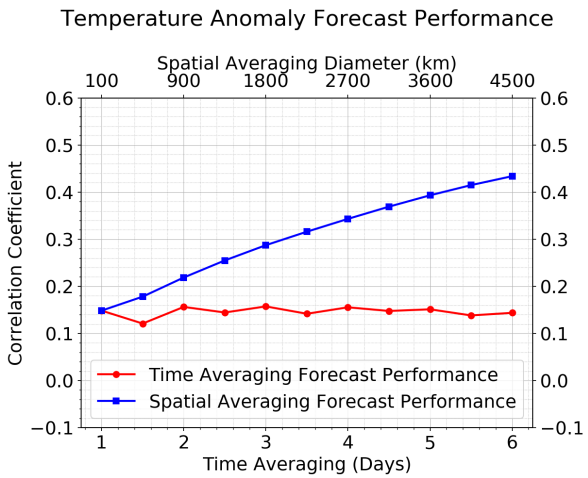

Figure S3: Effect of time and space averaging on forecast skill, averaged globally for surface temperature anomaly using the average from the past 14 days to the future 14 days as the seasonal cycle, at a lead time of 7 days.

1.3 Temperature anomaly data analysis using past 14 days average as the seasonal cycle

To avoid using the future information in the seasonal cycle, a version of seasonal cycle only using the past 14 days is implemented here as another robustness test for 3.5 months surface temperature data. The plots are still showing the spatial averaging is helping more than time averaging in most of the locations globally.

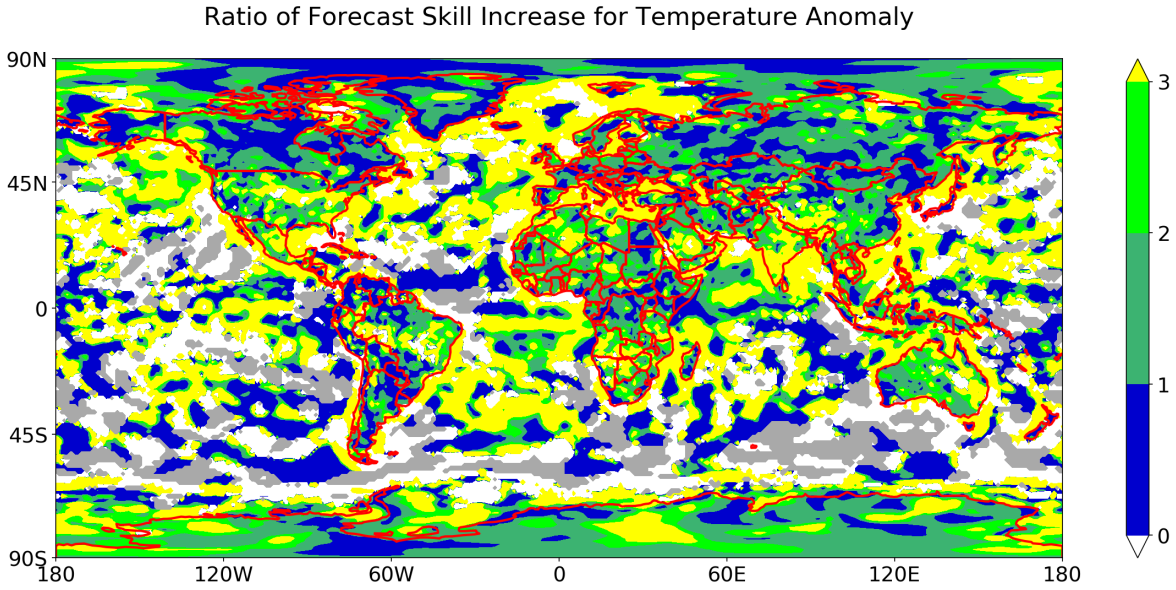

Figure S4: Global map of the ratio of forecast skill increase, defined as $r = \Delta_x\rho/\Delta_t\rho$, where $\Delta_x\rho$ is the change in forecast skill due to increased spatial averaging, and $\Delta_t\rho$ is the change in forecast skill for increased time averaging for surface temperature anomaly using the average from the past 14 days to the present as the seasonal cycle.

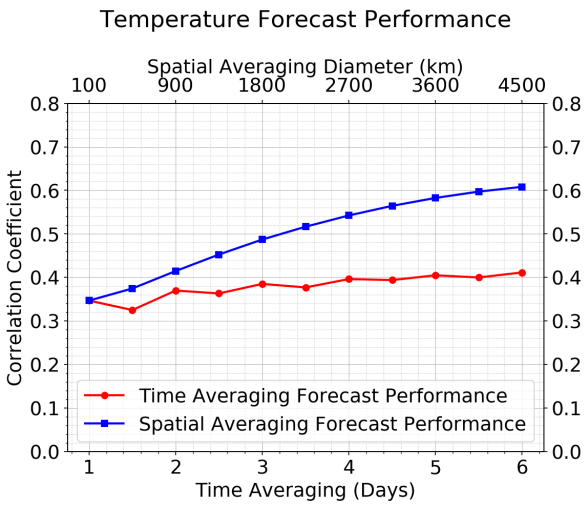

Figure S5: Effect of time and space averaging on forecast skill, averaged globally for surface temperature anomaly using the average from the past 14 days to the present as the seasonal cycle, at a lead time of 7 days.

1.4 Assessing tropical precipitation forecast skills using GPM data

In the main text, the truth signal was taken to be the day-0 analysis from the GFS model. Here, as an additional test, an observational data product is used as the truth signal instead of the model data product. In particular, GPM data is used to serve as the true precipitation data for testing the robustness as well. We compare the GFS precipitation forecast data, at a lead time of 3 days, to the GPM data to assess the forecast skill.

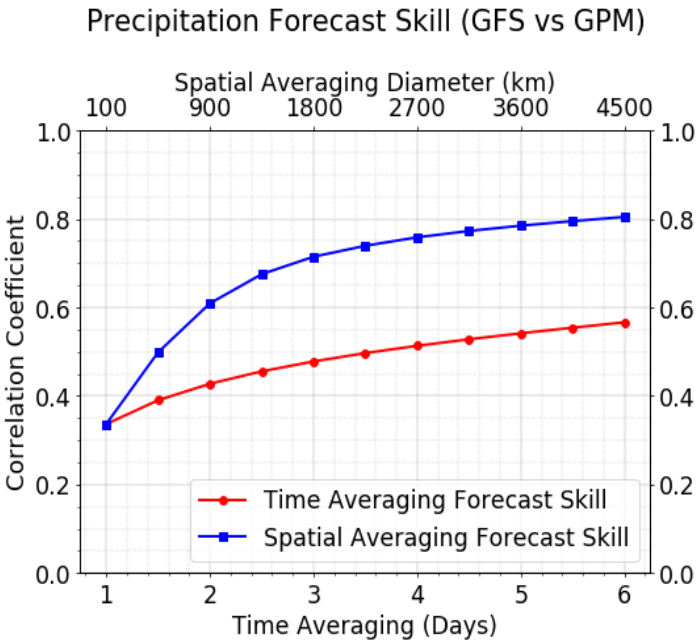

Figure S6: Effect of time and space averaging on forecast skill, averaged over tropical areas from 12°S to 12°N for comparing GFS precipitation rate forecast with GPM data, at a lead time of 3 days

Due to the GPM only having full observations from $60°S$ to $60°N$ while a maximum of 4500 km spatial averaging diameter is required in our analysis, the results of this additional test are limited to tropical locations from 12°S to 12°N, so that the entire spatial averaging disc is contained in the GPM data coverage from $60°S$ to $60°N$.

As seen in Fig. S6, it is again seen that spatial averaging outperforms time averaging in increasing forecast skill. One difference here is that, for short spatial/time averaging, the tropical averaged precipitation rate forecast skills are lower than the global averaged ones shown in the main text. This is within expectation based on earlier work since tropical precipitation has less predictability than extratropical precipitation. This additional test can also be taken as a special case of analyzing one region (i.e., the tropics), and again the main conclusion is robust: spatial averaging improves forecast skills more than time averaging.

2 Analytic Formulas for Decorrelation Time

In this section, we present the derivation of the analytic formula for the decorrelation time, including the decorrelation time of the time-averaged process. In the calculation, we use a continuous-time version of the AR(1) model called the Ornstein–Uhlenbeck (OU) process.

The Ornstein-Uhlenbeck process is defined as

$$du(t) = -\frac{u(t)}{T_d}dt + \sigma dW(t) \tag{S1}$$

with positive parameters $T_d, \sigma > 0$ and $dW(t)$ is related to a Gaussian white noise $\dot{W}(t)$ via

$$dW(t) = \dot{W}(t)dt, \tag{S2}$$

that is, white noise is a "derivative" of the Winener process $W(t)$ and it satisfies the following properties

$$\mathbb{E}[\dot{W}(t)] = 0, \tag{S3}$$
$$\mathbb{E}[\dot{W}(t)\dot{W}(s)] = \delta(t-s). \tag{S4}$$

The exact solution of (S2) is

$$u(t) = e^{-t/T_d}u(0) + \sigma\int_0^t e^{-(t-s)/T_d}dW(s) \tag{S5}$$

As $t \to \infty$, or as the initial time tends to $-\infty$, $u(t)$ will converge to a stationary Gaussian distribution with mean 0 and variance $\sigma^2 T_d/2$ [1, 3]. In what follows, we consider the stochastic process in its stationary state.

For the definition of the time averaged signal $\bar{u}(t)$, we use the values of $u(t)$ averaged over a centered time-averaging window with length T_w, so the averaged signal is defined as

$$\bar{u}(t) = \frac{1}{T_w}\int_{t-T_w/2}^{t+T_w/2} u(s)ds \tag{S6}$$

To define the decorrelation time $\overline{T}_d$, we use the auto-correlation function, $ACF(\tau) = \mathbb{E}[\overline{u}(t)\overline{u}(t+\tau)]/\mathrm{var}[\overline{u}(t)] = \overline{C}(\tau)/\overline{C}(0)$ for time lag τ where $\overline{C}(\tau)$ is the auto-covariance function for lag τ. Then the analytic formula for the de-correlation time of $\overline{u}(t)$ is defined as

$$\begin{aligned}\overline{T}_d &= \int_0^\infty ACF(\tau)d\tau \\ &= \int_0^\infty \frac{\overline{C}(\tau)}{\overline{C}(0)}d\tau \\ &= \frac{\int_0^\infty \overline{C}(\tau)d\tau}{\overline{C}(0)}.\end{aligned} \tag{S7}$$

The next goal is to find the formula for $\overline{C}(\tau)$. To do this, it is convenient to re-write the definition

of $\overline{u}(t)$ as

$$\begin{aligned}\bar{u}(t) &= \frac{1}{T_w}\int_{t-T_w/2}^{t+T_w/2} u(s)ds \\ &= \frac{1}{T_w}\int_{-\infty}^{\infty} u(s)\mathbb{1}_{[t-T_w/2,t+T_w/2]}(s)ds \\ &= \int_{-\infty}^{\infty} u(\alpha)g(t-\alpha)d\alpha \\ &= (g*u)(t)\end{aligned} \tag{S8}$$

where $\mathbb{1}(t)$ is the indicator function and $g(t) = \frac{1}{T_w}\mathbb{1}_{[-T_w/2,T_w/2]}(t)$. Hence, this expresses $\bar{u}(t)$ as a convolution between the original signal $u(t)$ and a rectanglar function $g(t)$. By now transforming to Fourier space, the convolution will become a multiplication and allow several useful formulas to be obtained:

$$\begin{aligned}\widehat{\overline{u}}_\nu &= \widehat{g}_\nu \widehat{u}_\nu, \\ |\widehat{\overline{u}}_\nu|^2 &= |\widehat{g}_\nu|^2 |\widehat{u}_\nu|^2, \\ E|\widehat{\overline{u}}_\nu|^2 &= |\widehat{g}_\nu|^2 \cdot \mathbb{E}|\widehat{u}_\nu|^2, \\ \widehat{\overline{C}}(\nu) &= \widehat{G}(\nu)\cdot\widehat{C}(\nu)\end{aligned} \tag{S9}$$

$$\begin{aligned}\widehat{G}(\nu) = |\widehat{g}(\nu)|^2 &= |\int_{-\infty}^{\infty} \frac{1}{T_w} 1_{[-T_w/2,T_w/2]}(x) e^{-2\pi x\nu i}dx|^2 \\ &= |\frac{1}{T_w}\int_{-T_w/2}^{T_w/2} e^{-2\pi x\nu i}dx|^2 \\ &= |\frac{1}{-2\pi T_w \nu i}(e^{-\pi\nu T_w i} - e^{\pi\nu T_w i})|^2 \\ &= |\frac{1}{2\pi T_w\nu} i(\cos(\pi\nu T_w) - i\sin(\pi\nu T_w) - \cos(\pi\nu T_w) - i\sin(\pi\nu T_w))|^2 \\ &= |\frac{1}{\pi T_w \nu}\sin(\pi\nu T_w)|^2 \\ &= \frac{\sin^2(\pi T_w\nu)}{\pi^2 T_w^2 \nu^2}\end{aligned} \tag{S10}$$

From these expressions, one can see that the problem of finding $\overline{C}(\tau)$ is equivalent to the problem of finding $\hat{\overline{C}}(\nu)$, since the two quantities are related by a Fourier transform.

To find an analytic expression for $\widehat{\overline{C}}(\nu)$, we start from the definition of the OU process to find $\hat{u}_\nu$:

$$\begin{aligned}\frac{du(t)}{dt} &= -u_t/T_d + \sigma\dot{W}_t \\ \int_{-\infty}^{\infty}\frac{du(t)}{dt}e^{-2\pi i\nu t}dt &= -\hat{u}_\nu/T_d + \sigma\widehat{\dot{W}}_\nu \\ u(t)e^{-2\pi i\nu t}|_{-\infty}^{\infty} + 2\pi i\nu\int_{-\infty}^{\infty} u(t)e^{-2\pi i\nu t}dt &= -\hat{u}_\nu/T_d + \sigma\widehat{\dot{W}}_\nu \\ 2\pi i\nu\hat{u}_\nu &= -\hat{u}_\nu/T_d + \sigma\widehat{\dot{W}}_\nu \\ \hat{u}_\nu &= \frac{\sigma\widehat{\dot{W}}_\nu}{1/T_d + 2\pi\nu i}\end{aligned} \tag{S11}$$

$$\begin{aligned}\mathbb{E}[\widehat{u}_\nu\widehat{u}^*_{\nu'}] &= \frac{\sigma}{1/T_d + 2\pi\nu i}\cdot\frac{\sigma}{1/T_d - 2\pi\nu' i}\mathbb{E}[\widehat{\dot{W}}_\nu\widehat{\dot{W}}^*_{\nu'}] \\ &= \frac{\sigma^2}{1/T_d^2 + 4\pi^2\nu^2}\delta(\nu-\nu')\end{aligned} \tag{S12}$$

Hence

$$\widehat{C}(\nu) = \frac{\sigma^2}{1/T_d^2 + 4\pi^2\nu^2} \tag{S13}$$

By the equality in (S9),

$$\widehat{\overline{C}}(\nu) = \widehat{G}(\nu) \cdot \widehat{C}(\nu) = \frac{\sin^2(\pi T_w \nu)}{\pi^2 T_w^2 \nu^2} \frac{\sigma^2}{1/T_d^2 + 4\pi^2\nu^2} \tag{S14}$$

Returning now to $\overline{C}(\tau)$, the numerator $\int_0^\infty \overline{C}(\tau)d\tau$ in the definition of the decorrelation time (7) can be derived as

$$\begin{aligned}
\int_0^\infty \overline{C}(\tau)d\tau &= \frac{1}{2}\int_{-\infty}^{\infty} \overline{C}(\tau)d\tau \\
&= \frac{1}{2}\int_{-\infty}^{\infty} \overline{C}(\tau)e^{-2\pi i\nu\tau}d\tau\Big|_{\nu=0} \\
&= \frac{1}{2}\widehat{\overline{C}}(\nu = 0) \\
&= \frac{1}{2}\lim_{\nu\to 0}\widehat{\overline{C}}(\nu) \\
&= \frac{1}{2}\lim_{\nu\to 0}\frac{\sin^2(\pi T_w\nu)}{\pi^2 T_w^2\nu^2}\frac{\sigma^2}{1/T_d^2 + 4\pi^2\nu^2} \\
&= \frac{\sigma^2 T_d^2}{2}
\end{aligned} \tag{S15}$$

Then what remains needed from (S7) is the denominator, $\overline{C}(0)$. From the equation (52) in the paper [2], for a complex-valued OU process, the variance of the time avaraged signal has been calcuated. By taking the $\gamma = 1/T_d$ and $\omega = 0$, the auto-covariance function for the averaged real-valued OU process can be found as

$$\overline{C}(0) = \frac{\sigma^2 T_d^3}{T_w^2}(T_w/T_d - 1 + e^{-T_w/T_d}) \tag{S16}$$

Finally, from the definition of the decorrelation time in (S7), we find

$$\begin{aligned}
\overline{T}_d &= \frac{\int_0^\infty \overline{C}(\tau)d\tau}{\overline{C}(0)} \\
&= \frac{\sigma^2 T_d^2/2}{\frac{\sigma^2 T_d^3}{T_w^2}(T_w/T_d - 1 + e^{-T_w/T_d})} \\
&= T_d \cdot \frac{(T_w/T_d)^2}{2(T_w/T_d - 1 + e^{-T_w/T_d})},
\end{aligned} \tag{S17}$$

which is the desired result of an analytic expression for the decorrelation time of the time-averaged process $\overline{u}(t)$.

As a consistency check, it can be verified that, for the original unaveraged signal $u(t)$, the decorrelation time is just T_d; to see this, take the limit $T_w \to 0$ in (S17) to see that

$$\begin{aligned}
\lim_{T_w\to 0}\overline{T}_d &= \lim_{T_w\to 0} T_d \cdot \frac{(T_w/T_d)^2}{2(T_w/T_d - 1 + 1 - T_w/T_d + \frac{(T_w/T_d)^2}{2} + O(T_w^3))} \\
&= T_d \lim_{T_w\to 0}\frac{(T_w/T_d)^2}{(T_w/T_d)^2 + O(T_w^3)} \\
&= T_d.
\end{aligned}$$

Furthermore, a simpler, approximate version of (S17) can be derived as follows, assuming that T_w/T_d

is small:

$$\begin{aligned}
\overline{T}_d &= T_d \cdot \frac{(T_w/T_d)^2}{2(T_w/T_d - 1 + e^{-T_w/T_d})} \\
&= T_d \cdot \frac{(T_w/T_d)^2}{2(T_w/T_d - 1 + (1 - T_w/T_d + \frac{(T_w/T_d)^2}{2!} - \frac{(T_w/T_d)^3}{3!} + O((T_w/T_d)^4))} \\
&= T_d \cdot \frac{(T_w/T_d)^2}{(T_w/T_d)^2 - \frac{1}{3}(T_w/T_d)^3 + O((T_w/T_d)^4)} \\
&= T_d \cdot \frac{1}{1 - \frac{1}{3}(T_w/T_d) + O((T_w/T_d)^2)} \\
&= T_d(1 + \frac{1}{3}(T_w/T_d) + O((T_w/T_d)^2)) \\
&= T_d + \frac{1}{3}T_w + T_d \cdot O(T_w^2/T_d^2)
\end{aligned} \tag{S18}$$

For small T_w/T_d, equation (S18) leads to

$$\overline{T}_d \approx T_d + \frac{1}{3}T_w. \tag{S19}$$

3 Performance increase in terms of percentages

In the main text in Figures 3–6 we have shown how the absolute correlation coefficient in a forecast changes when different time averaging windows and spatial avearging windows are applied. Some of the locations have very good performance skill already when no averaging is used, especially for surface temperature. It is therefore also informative to show the percentage increase in the correlation coefficient when time/space averaging is applied with respect to the baseline (1-day averaging and 100km spatial averaging). These figures are shown here as Figures S7–S10.

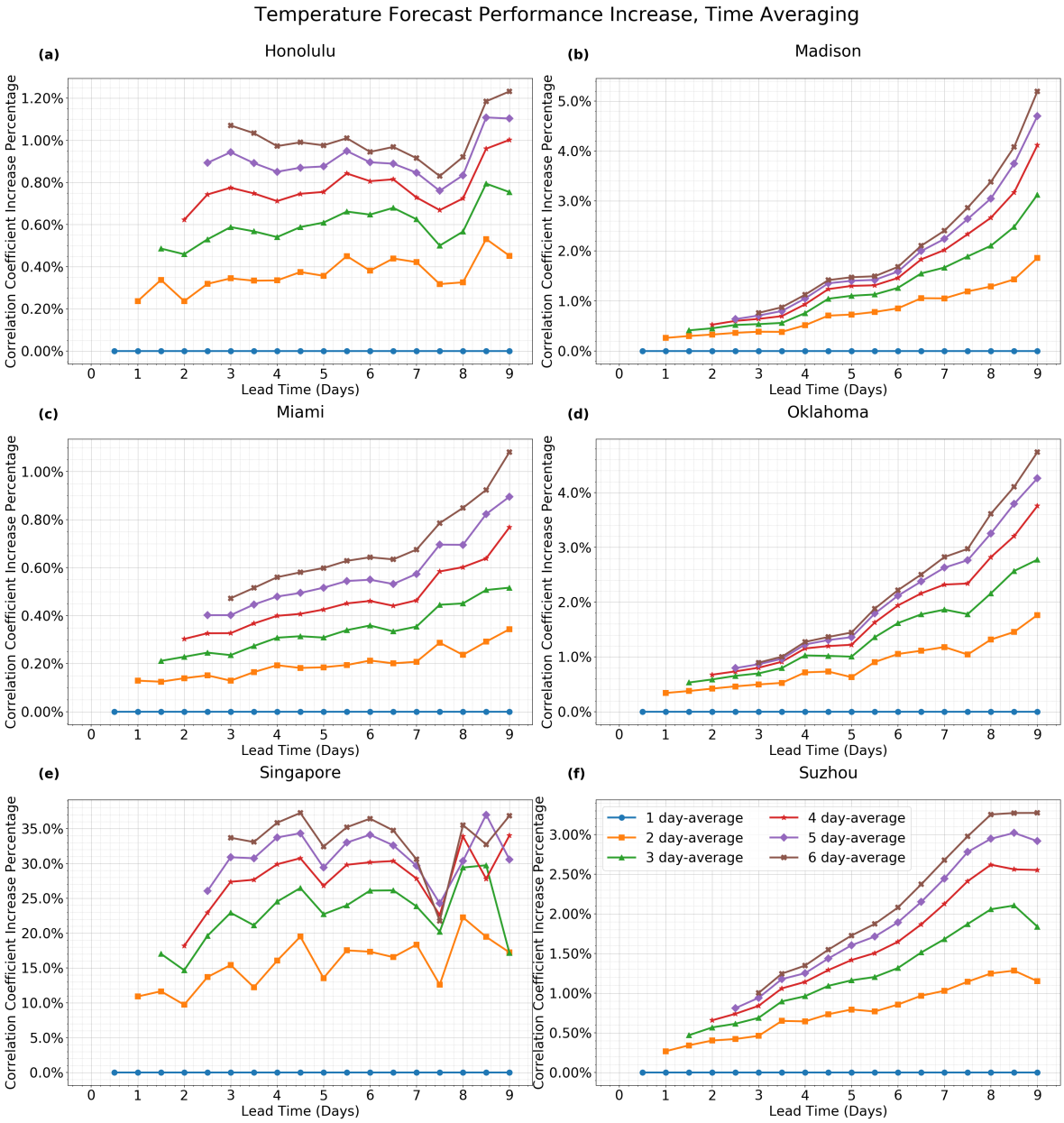

Figure S7: Effects of time averaging on forecast performance, for surface temperature, with 100-km spatial averaging, at several locations around the globe: (a) Honolulu, Hawaii ($21°N, 158°W$), (b) Madison, Wisconsin ($43°N, 89°W$), (c) Miami, Florida ($26°N, 80°W$), (d) Oklahoma City, Oklahoma ($35°N, 98°W$), (e) Singapore ($1°N, 104°E$), and (f) Suzhou, China ($31°N, 120°E$). Performance percentage change is calculated by comparing to the baseline skill with 1-day time averaging and 100-km spatial averaging.

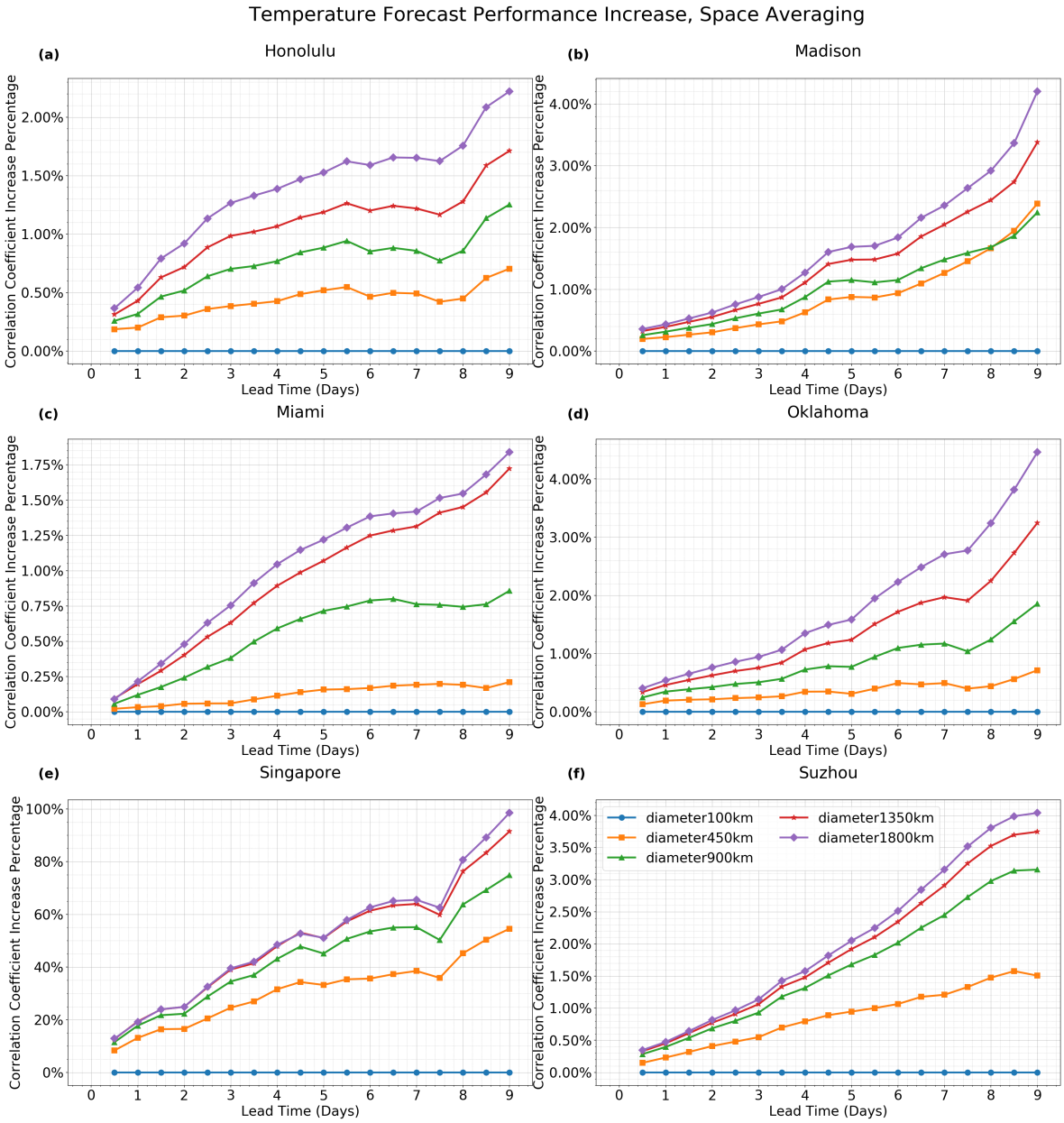

Figure S8: Effects of spatial averaging on forecast performance, for surface temperature, with 100-km spatial averaging, at several locations around the globe: (a) Honolulu, Hawaii ($21°N, 158°W$), (b) Madison, Wisconsin ($43°N, 89°W$), (c) Miami, Florida ($26°N, 80°W$), (d) Oklahoma City, Oklahoma ($35°N, 98°W$), (e) Singapore ($1°N, 104°E$), and (f) Suzhou, China ($31°N, 120°E$). Performance percentage change is calculated by comparing to the baseline skill with 1-day time averaging and 100-km spatial averaging.

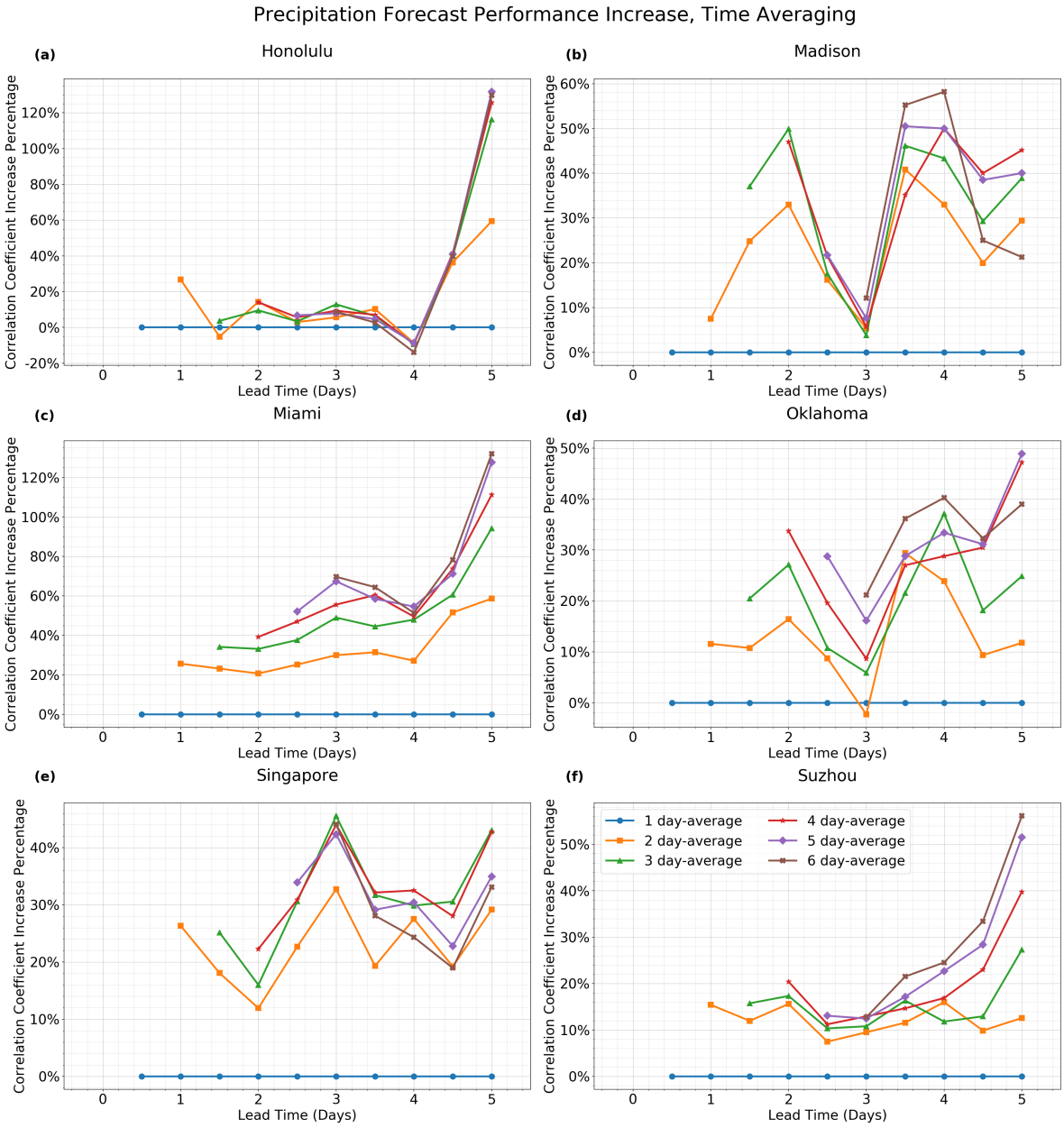

Figure S9: Effects of time averaging on forecast performance, for precipitation, with 100-km spatial averaging, at several locations around the globe: (a) Honolulu, Hawaii ($21°N, 158°W$), (b) Madison, Wisconsin ($43°N, 89°W$), (c) Miami, Florida ($26°N, 80°W$), (d) Oklahoma City, Oklahoma ($35°N, 98°W$), (e) Singapore ($1°N, 104°E$), and (f) Suzhou, China ($31°N, 120°E$). Performance percentage change is calculated by comparing to the baseline skill with 1-day time averaging and 100-km spatial averaging.

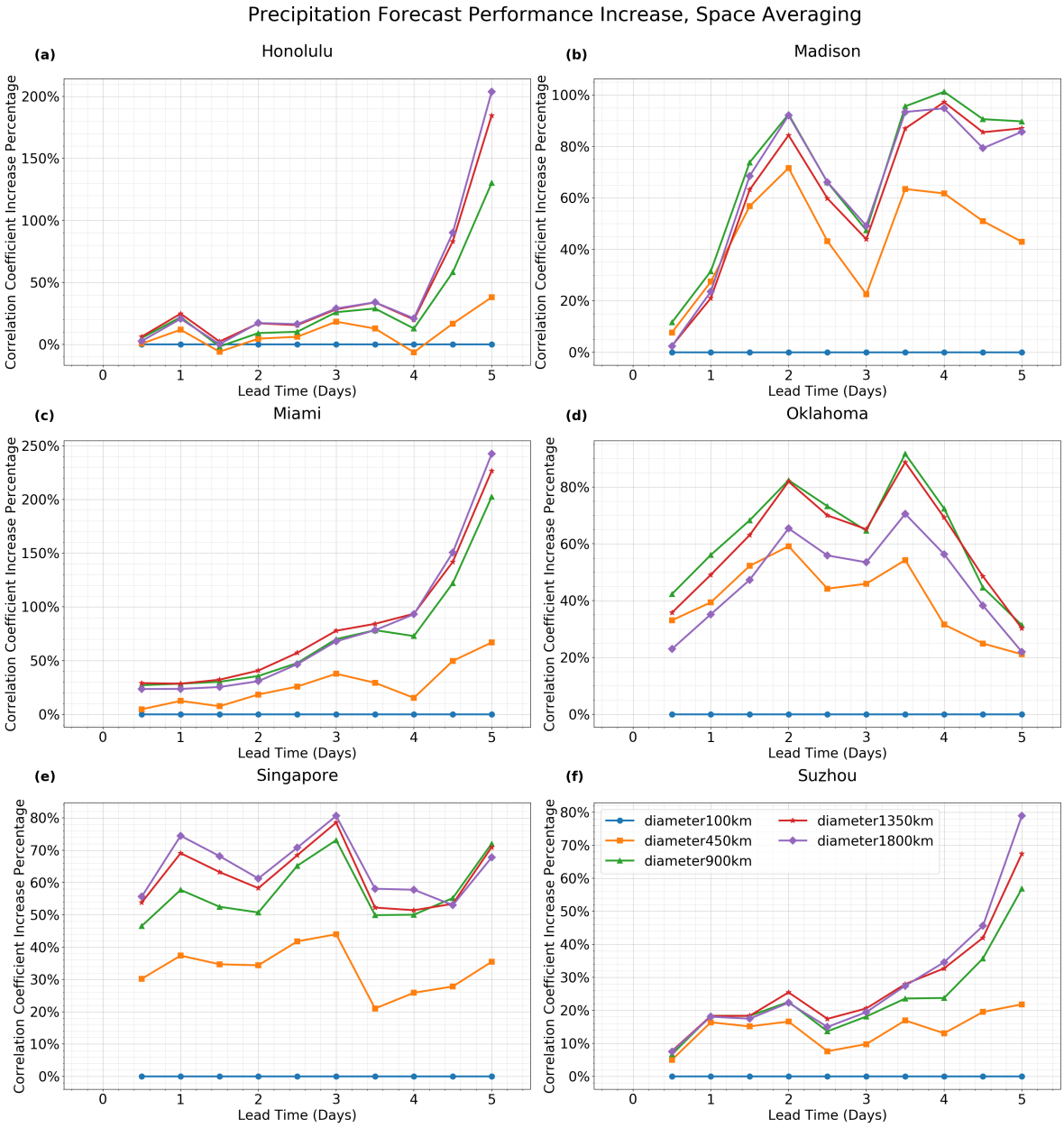

Figure S10: Effects of spatial averaging on forecast performance, for precipitation, with 100-km spatial averaging, at several locations around the globe: (a) Honolulu, Hawaii ($21°N, 158°W$), (b) Madison, Wisconsin ($43°N, 89°W$), (c) Miami, Florida ($26°N, 80°W$), (d) Oklahoma City, Oklahoma ($35°N, 98°W$), (e) Singapore ($1°N, 104°E$), and (f) Suzhou, China ($31°N, 120°E$). Performance percentage change is calculated by comparing to the baseline skills with 1-day time averaging and 100-km spatial averaging.

References

[1] C. W. Gardiner. *Handbook of stochastic methods: for physics, chemistry & the natural sciences*, volume 13 of *Springer Series in Synergetics*. Springer–Verlag, Berlin, 2004.

[2] Y. Li and S. N. Stechmann. Spatial and temporal averaging windows and their impact on forecasting: exactly solvable examples. *Math. Clim. Weather Forecast.*, 4:23–49, 2018.

[3] A. J. Majda and J. Harlim. *Filtering Turbulent Complex Systems*. Cambridge University Press, 2012.